ACS APPLIED MATERIALS & INTERFACES

Research Article

www.acsami.org

Hybrid Phototransistors Based on Bulk Heterojunction Films of Poly(3-hexylthiophene) and Zinc Oxide Nanoparticle

Sungho Nam,[†] Jooyeok Seo,[†] Soohyeong Park,[†] Sooyong Lee,[†] Jaehoon Jeong,[†] Hyena Lee,[†] Hwajeong Kim,*[,†,‡] and Youngkyoo Kim*[,†]

[†]Organic Nanoelectronics Laboratory, Department of Chemical Engineering, and [‡]Research Institute of Advanced Energy Technology, Kyungpook National University, Daegu 702-701, Republic of Korea

Supporting Information

ABSTRACT: Hybrid phototransistors (HPTRs) were fabricated on glass substrates using organic/inorganic hybrid bulk heterojunction films of p-type poly(3-hexylthiophene) (P3HT) and n-type zinc oxide nanoparticles (ZnO_{NP}). The content of ZnO_{NP} was varied up to 50 wt % in order to understand the composition effect of ZnO_{NP} on the performance of HPTRs. The morphology and nanostructure of the P3HT:ZnO_{NP} films was examined by employing high resolution electron microscopes and synchrotron radiation grazing angle X-ray diffraction system. The incident light intensity (P_{IN}) was varied up to 43.6 $\mu W/cm^2$, whereas three major wavelengths (525 nm, 555 nm, 605 nm) corresponded to the optical absorption of P3HT were applied. Results showed that the present HPTRs showed typical p-type transistor performance even though the n-type ZnO_{NP} content increased up to 50 wt %. The highest transistor performance was obtained at 50 wt %, whereas the lowest performance was measured at 23 wt % because of the immature bulk heterojunction morphology. The drain current (I_D) was proportionally increased with P_{IN} due to the photocurrent generation in addition to the field-effect current. The highest apparent and corrected responsivities (R_A = 4.7 A/W and R_C = 2.07 A/W) were achieved for the HPTR with the P3HT:ZnO_{NP} film (50 wt % ZnO_{NP}) at P_{IN} = 0.27 $\mu W/cm^2$ (555 nm).

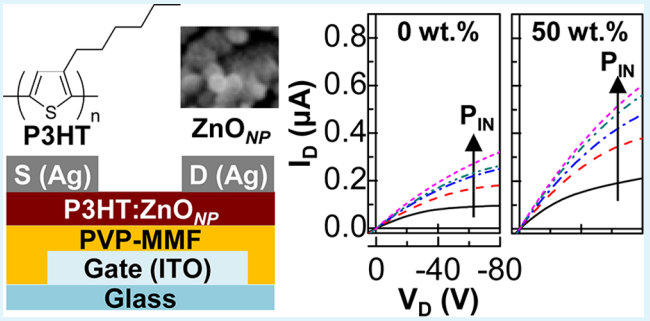

KEYWORDS: *hybrid phototransistors, P3HT, zinc oxide nanoparticles, organic/inorganic bulk heterojunction, morphology, responsivity*

INTRODUCTION

For the last two decades, organic semiconductors have been extensively studied because of their particular features such as low-temperature processes, easy tuning of band gap energy by chemical synthesis, possible fabrication of various device/module shapes, and low-cost manufacturing of large-scale and flexible devices compared to conventional inorganic semiconductors.[1−5] The first fruitful commercial products using organic semiconductors are organic light-emitting devices (OLED) for display applications.[6−8] Then the coverage of organic semiconductor researches has been extended to organic solar cells (OSC), organic memory devices (OMD), organic field-effect transistors (OFET), organic photodiodes (OPD), and organic phototransistors (OPTR).[9−24] Of these various applications, the OPTR research has not been seriously highlighted, even though OPTRs have a great merit as an ultrathin-lightweight-flexible photodetector because they can be fabricated on plastic film substrates at room temperature.[22−25]

To date, various organic semiconductors including small molecules and polymers have been used for OPTRs.[26−36] In particular, extremely high responsivities (300−4300 A/W)[37−39] have been reported for some materials, which may require further calibration because quantum efficiency (QE) cannot be theoretically higher than 100% when it comes to the relation, QE ≈ $1240R_C/\lambda$, where R_C and λ are the corrected responsivity (that is calculated after subtracting the field-effect current under dark condition from the overall current under light illumination) and the wavelength of incident light in nm:[40] Here we should bear in mind that the photocurrent generation is in principle restricted for the field-effect zone in the channel layer, because the field-effect zone is already excited by the electric field, but it is possible to efficiently collect the photogenerated charges due to the source-drain electric field.[33] For example, the theoretical maximum R_C can be calculated as ∼40 A/W at the wavelength of 500 nm. On this account, using pristine organic semiconductors (either p-type or n-type) solely is considered inefficient for the OPTR applications because the (individual) charge generation/separation yield is basically low owing to the absence of appropriate driving forces such as electron donor−acceptor systems even if the exciton formation yield (before charge separation) can be high. In this regard, bulk heterojunction

Received: November 20, 2012
Accepted: January 25, 2013
Published: February 12, 2013

(BHJ) films, such as blends of *p*-type polymers and *n*-type small molecules, blends of *p*-type polymers and *n*-type polymers, and composites of polymers and inorganic nanoparticles, have been recently introduced as the channel layer in the OPTRs.[32−35]

Of these BHJ type OPTRs, composite films of *p*-type polymers and *n*-type inorganic nanoparticles, which can lead to hybrid phototransistors (HPTRs), are expected to be advantageous in terms of device stability due to the stronger nature of inorganic materials than organic materials. However, only one study, which is based on the composite film of poly(3-hexylthiophene) (P3HT) and titanium oxide (TiO_2), has been attempted for HPTRs but the accurate responsivity was not investigated in detail.[41] We note that a P3HT/soluble fullerene-based OPTR with lead sulfide (PbS) nanoparticles has been reported but this approach was fundamentally different from HPTRs[34] and that a hybrid transistor based on the composite films of poly(2-methoxy-5-(2-ethylhexyloxy)-1,4-phenylenevinylene) (MEH-PPV)/zinc oxide (ZnO) nanocrystals has been reported but it was not for HPTR but just for simple transistors.[42] Thus no actual study has been reported for HPTRs with composite films of *p*-type polymer and *n*-type zinc oxides (ZnO), even though ZnO materials are cheap and their energy band structure is well-fitted for efficient charge separation with *p*-type polymers.[43]

In this work, we have fabricated HPTRs with composite films of P3HT and ZnO nanoparticles (ZnO_{NP}) by varying the ZnO_{NP} compositions up to 50 wt % in order to examine the influence of ZnO_{NP} contents on the performance of HPTRs. In addition, the wavelength and intensity of incident light into the HPTRs has been varied for the investigation of intensity-dependent and/or wavelength-dependent responsivity changes. Results showed that the apparent responsivity of the P3HT:ZnO_{NP} HPTRs has reached ∼4.7 A/W at the wavelength of 555 nm (R_C ≈ 2.07 A/W at the incident light intensity of ∼0.27 $\mu W/cm^2$) when the ZnO_{NP} composition was 50 wt %.

EXPERIMENTAL SECTION

Materials and Solutions. P3HT polymer (regioregularity = 95%, weight-average molecular weight = 6.0×10^4, polydispersity index = 2.0) was purchased from Lumtec (Taiwan) and used without further purification. ZnO_{NP} (purity = 99.5%, average particle size = 20 nm) was supplied from Nano Amor, Inc. (USA). Poly(vinylphenol) (PVP) and methylated poly(melamine-co-formaldehyde) (MMF) were received from Sigma-Aldrich. Silver metals were purchased from Sigma-Aldrich and used for the deposition of source and drain electrodes. Pristine and binary blend solutions of P3HT and ZnO_{NP} were prepared by varying the ZnO_{NP} contents (0, 9, 23, 33, 43, 50 wt %) in cosolvents of chlorobenzene (CB) and methanol (MeOH) (CB:MeOH = 95:5 by volume) at a solid concentration of 15 mg/mL. MeOH was used as a dispersion agent for ZnO_{NP}. These solutions were stirred vigorously on a hot plate before spin-coating process. The PVP-MMF solution (PVP:MMF = 1:1.25) was prepared in propylene glycol monomethyl ether acetate (PGMEA) at a solid concentration of 100 mg/mL.[44]

Thin Film and Device Fabrication. Prior to device fabrication, indium tin oxide (ITO)-coated glass substrates (∼10 Ω/cm^2) were subject to photolithography/etching processes to form the ITO stripe of 1 mm ×12 mm for the use of gate electrodes. The patterned ITO-glass substrates were cleaned using acetone and isopropyl alcohol, followed by drying with a nitrogen flow. The PVP-MMF solution was spin-coated on top of the cleaned ITO-coated glass substrates, followed by prebaking at 120 °C for 10 min and thermal cross-linking at 220 °C for 60 min. The thickness of the PVP-MMF gate insulator films was ∼700 nm. On top of the PVP-MMF layers, pristine P3HT solutions or blend solutions (P3HT:ZnO_{NP}) were spin-coated and soft-baked at 60 °C for 15 min. These samples were loaded into a vacuum chamber equipped inside an argon-filled glovebox system. Then Ag metals were thermally evaporated through a metal shadow mask in a vacuum of ∼1×10^{-6} Torr to make source-drain (S-D) electrodes, which defined the channel length of L = 70 μm and the channel width of W = 3 mm ($W/L \approx 42.8$). The fabricated devices were stored inside the argon-filled glovebox in order to protect them from moisture and oxygen before measurements. The device structure is shown in Figure 1.

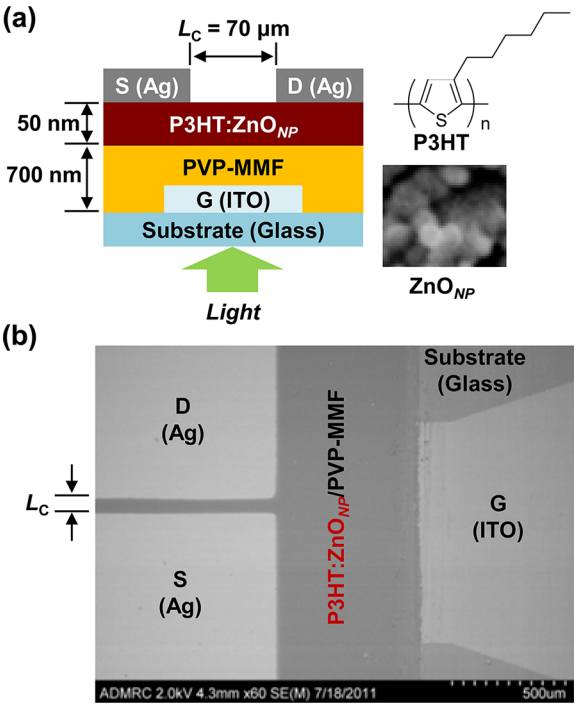

Figure 1. (a) Schematic illustration of hybrid phototransistor (HPTR) with the P3HT:ZnO_{NP} films, (b) SEM image (top view) for the HPTR fabricated in this work. *S*, *D*, *G*, and L_C denote source electrode, drain electrode, gate electrode, and channel length, respectively.

Measurements. The transistor characteristics were measured using a semiconductor parameter analyzer (Keithley SCS-4200). For the measurement of phototransistor characteristics the channel area was illuminated with a monochromatic light filtered from a Tungsten-Halogen lamp (150 W, ASBN-W, Spectral Products) using a monochromator (CM110, Spectral Products). The incident light intensity (P_{IN}) was measured with a calibrated Si photodiode (BS-520, AIST, Japan), while the film thickness was measured using a surface profiler (Alpha Step 200, Tencor). The optical absorption spectra of films were measured using a UV−visible spectrophotometer (Optizen 2120UV, Mecasys). The nanostructure of the P3HT:ZnO_{NP} blend films was measured using a synchrotron radiation grazing incidence angle X-ray diffraction (GIXD, wavelength = 0.1114 nm) system (Pohang Accelerator Laboratory, Republic of Korea) and high resolution transmission electron microscope (HR-TEM, Tecnai G2 F20 S-TWIN, Philips). The X-ray diffraction pattern of the ZnO_{NP} powders was measured using a X-ray diffractometer (MP-XRD, X'Pert PRO MPD, wavelength = 0.154 nm). The cross sections of devices and the film surfaces were measured using a scanning electron microscope (SEM, S-4800, Hitachi).

RESULTS AND DISCUSSION

The HPTRs with the P3HT:ZnO_{NP} active layers were fabricated as shown in Figure 1. Before moving to the experimental results, we need to briefly discuss the operating

mechanism of the present P3HT:ZnO_{NP} OPTR. As shown in Figure 2a, the energy offset (1.4 eV) between the lowest

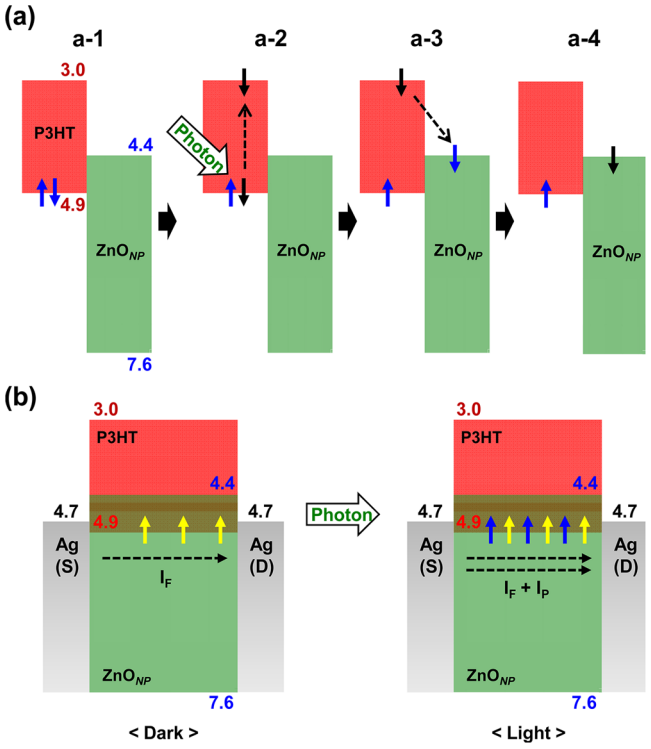

Figure 2. (a) Schematic illustration for the mechanism of charge generation and separation in the bulk heterojunction of the P3HT:ZnO_{NP} films upon illumination: (a-1) before illumination, (a-2) exciton generation upon illumination, (a-3) charge separation, (a-4) after charge separation) (b) Illustration for the current flow in the HPTR with the P3HT:ZnO_{NP} films before and after illumination. I_F and I_P denote field-effect current and photocurrent, respectively. Note that flat energy band diagrams without any energy band alignment by contact were considered for simplicity, while the unit (eV) and minus sign in the numbers was omitted to avoid crowding the diagrams.

unoccupied molecular orbital (LUMO = 3.0 eV) of P3HT and the conduction band (CB = 4.4 eV) of ZnO_{NP} is sufficiently large for the efficient charge separation from the excitons generated in the P3HT domains.[45−47] Thus, upon illumination, the electrons in the excitons (hole−electron pairs) of the P3HT domains can be easily transferred to the conduction band of ZnO_{NP} domains (see a-2 and a-3 in Figure 2a). Finally, the P3HT domains have holes in their HOMO levels (see a-4 in Figure 2a), which act as a charge carrier for generating photocurrents (I_P) upon field-effect operations in addition to the field-effect currents (I_F) (Figure 2b). Therefore, the overall currents in the present HPTRs can be sum of I_P and I_F upon illumination.

Next, we investigated the basic transistor characteristics of HPTRs without light illumination. As shown in Figure 3a, all HPTRs exhibited typical p-type output characteristics because the drain current (I_D) increased negatively as the gate voltage (V_G) increased negatively from 0 V to −80 V. Interestingly, we find that the I_D value at the same V_G was not linearly changed with the ZnO_{NP} content but showed a minimum at 23 wt %. Considering that the P3HT content decreases by increasing the ZnO_{NP} content in the P3HT:ZnO_{NP} films at the same thickness, it is expected that the I_D value at the same V_G is gradually decreased as the ZnO_{NP} content increases because of

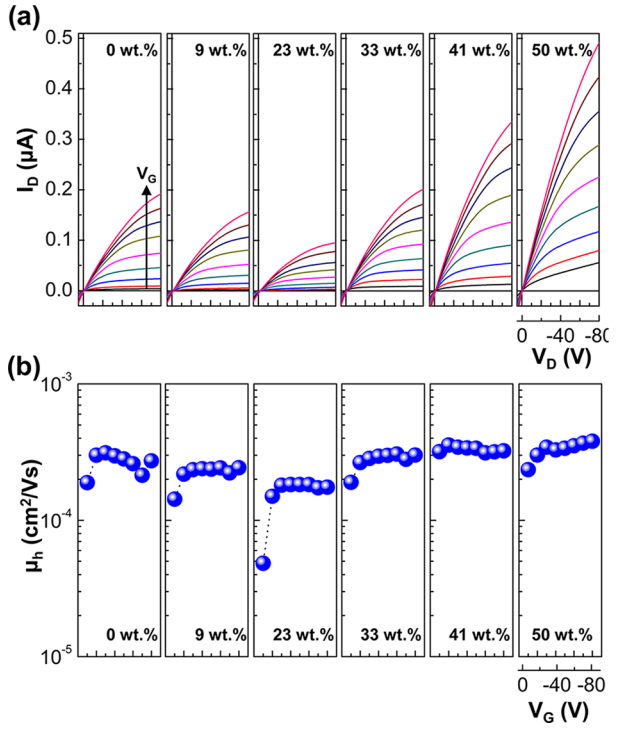

Figure 3. (a) Output curves of the HPTRs with the P3HT:ZnO_{NP} films in the dark (Arrow denotes the direction of V_G increase (negatively) from 0 V to −80 V, (b) hole mobility as a function of V_G at V_D = −80 V according to the ZnO_{NP} content.

the reduced amount of the P3HT excitons. The upturning I_D trend with the ZnO_{NP} content can be assigned to the slightly improved hole mobility (Figure 3b) which might be enabled by the presence of ZnO_{NP} of which surfaces act as a nucleating and anchoring site for P3HT chains to make better crystallization as observed in our previous report.[48] However, a close look at the output curves at V_G = 0 V provides us with the fact that there is a leakage current at higher ZnO_{NP} contents (see also transfer curves in Figure S1 in the Supporting Information). Hence both the improved hole mobility and the leakage current are considered to affect the upturning I_D trend at the ZnO_{NP} content between 23 and 33 wt %.

To further understand the abnormal output characteristics, we first examined the cross-section and surface parts of the P3HT:ZnO_{NP} layers in the HPTRs by employing a high-resolution SEM. As shown in Figure 4, the active layers seem to be formed well without a catastrophic defect even at higher ZnO_{NP} contents. We note that the embossed surface was similar for all samples but in the case of high ZnO_{NP} contents big nanoparticle-like domains were observed at the vicinity of the broken parts (see the circled parts in Figure 4a). Taking into account the average size of ZnO_{NP} (10−20 nm), the big domains at the edge parts are considered as ZnO_{NP} or its aggregates. The rough morphology of the P3HT:ZnO_{NP} films at high ZnO_{NP} contents was also measured using HRTEM as shown in Figure 4b. Therefore the leakage current in the HPTRs can be attributed to the rough morphology of the P3HT:ZnO_{NP} films at the high ZnO_{NP} contents because some metal parts of the top source and drain electrodes upon thermal evaporation could pass through pinholes created in the rough films.

For the investigation of possible nanoscopic changes in the P3HT stacking/ordering by the presence of ZnO_{NP}, the GIXD

dx.doi.org/10.1021/am302765a | ACS Appl. Mater. Interfaces 2013, 5, 1385−1392

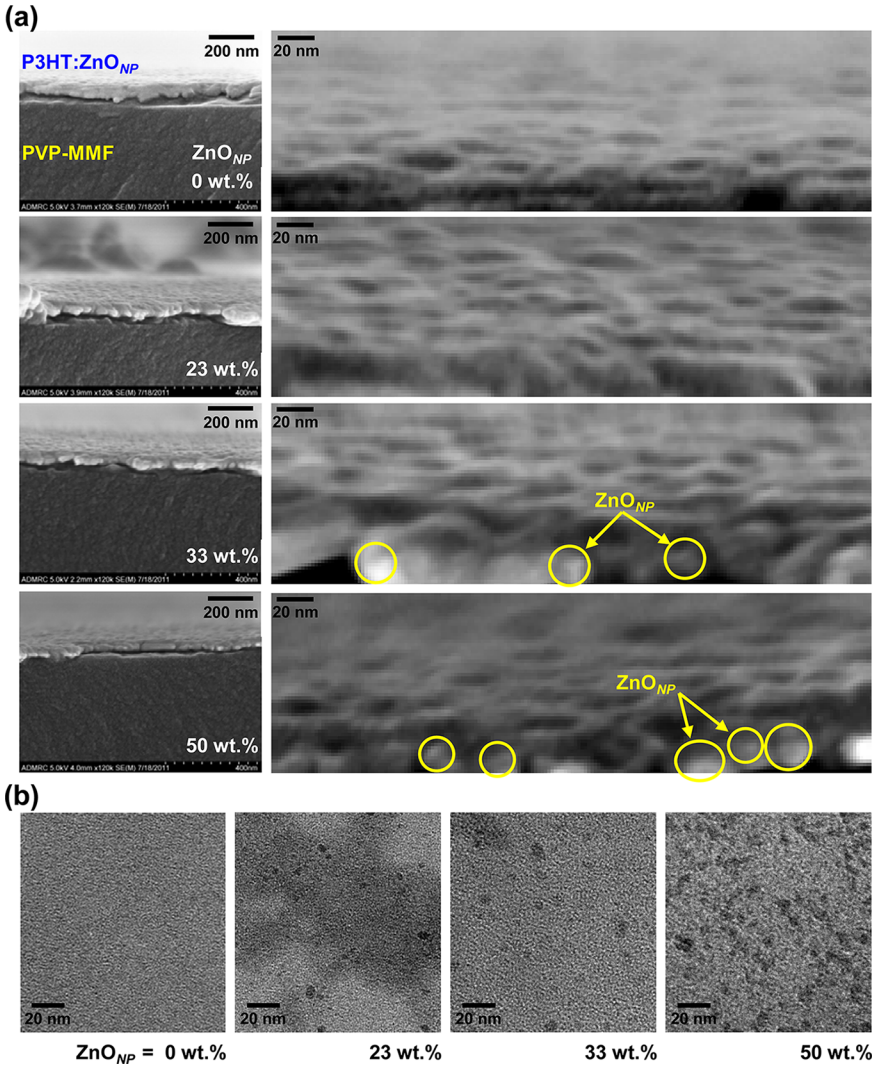

Figure 4. (a) SEM images for the cross-section parts (left) of the HPTRs with the P3HT:ZnO$_{NP}$ films and the enlarged images focusing on the P3HT:ZnO$_{NP}$ layers (right) (parts of ZnO$_{NP}$ and its aggregates are marked with circles). (b) TEM images for the P3HT:ZnO$_{NP}$ films.

measurements were carried out as shown in Figure 5. The 2D GIXD images in Figure 5a inform that the crystalline structure of films was noticeably changed, as the ZnO$_{NP}$ content increased, when it comes to the variation in the diffraction images (see also the enlarged images in Figure S2 in the Supporting Information). To look into the detailed parts, the 2D images were converted to corresponding 1D images. As shown in Figure 5b, the position of the P3HT main (100) diffraction peaks in the OOP direction was almost not changed with the ZnO$_{NP}$ content. In addition, the (200) peaks were also clearly measured without respect to the ZnO$_{NP}$ content. This result indicates that the ZnO$_{NP}$ did not severely destruct the P3HT crystalline structures, which can be attributed to the relatively large size of ZnO$_{NP}$ (ca. 10−20 nm) compared to the interchain distance (∼1.6 nm) of P3HTs in the OOP direction.[12,49−53] In the case of 1D profiles in the IP direction the (100) peak position was also unchanged and the peak intensity was quite small, indicative of less tendency of a-a stacking[12,49,50] in the IP direction. In addition, the (200) peaks were almost undetectable. This result reflects that most of P3HT chains in the P3HT:ZnO$_{NP}$ films, even at high ZnO$_{NP}$ contents, underwent preferred a-a stacking in the OOP direction. In other words, the b-b stacking, which corresponds to the interchain $\pi-\pi$ stacking geometry of P3HT, is predominant in the IP direction, which is advantageous for the present HPTRs because the charge transport occurs in the IP direction in the case of transistor operation. Here we note that the diffraction peaks of ZnO$_{NP}$ were obviously measured in both OOP and IP directions in the case of high ZnO$_{NP}$ contents (see Figure S3 in the Supporting Information for the powder XRD data of ZnO$_{NP}$ for reference but note that the position of peaks is slightly different between GIXD and power XRD data because of the different X-ray wavelengths as mentioned in the Experimental Section).

In addition to the fundamental aspect of P3HT chain stacking/ordering, we calculated the size of P3HT crystals from the (100) peaks of 1D profiles in Figure 5b,c. As shown in Figure 6a, the crystal size (L_{100}) in the IP direction was decreased as the ZnO$_{NP}$ content increased up to 33 wt % and then it was increased again by further addition of ZnO$_{NP}$. This trend is similar to the I_D trend in Figure 3a even though the minimum point here (33 wt %) is different from that in Figure 3a (23 wt %). The similar behavior is seen for the crystal size in the OOP direction, except the slightly high crystal size at 23 wt %. Thus the upturning I_D trend in the output curves (see Figure 3a) is considered to be closely related with the crystal sizes of

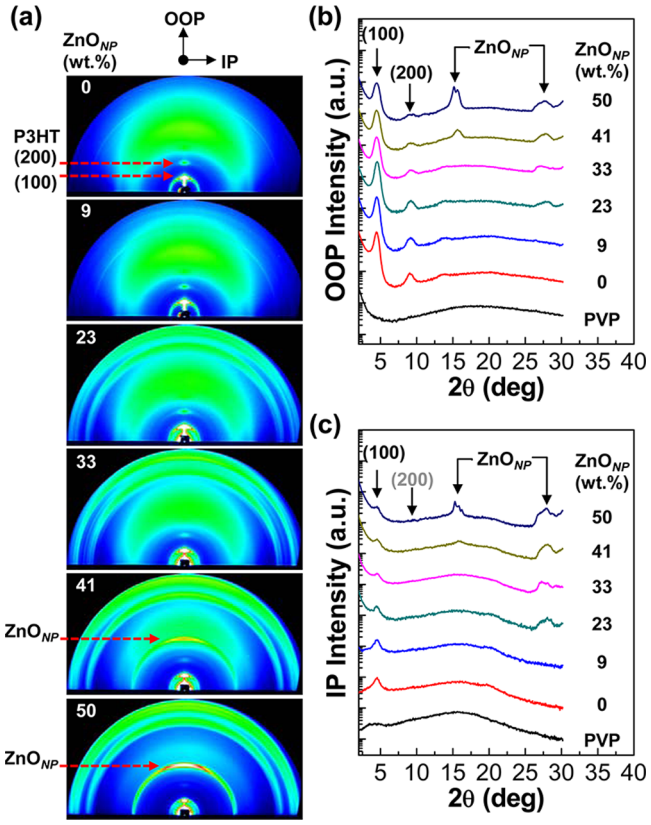

Figure 5. (a) 2D GIXD images of the P3HT:ZnO_{NP} films coated on the PVP-MMF/ITO-glass substrates, (b) 1D profiles in the OOP direction, and (c) 1D profiles in the IP direction.

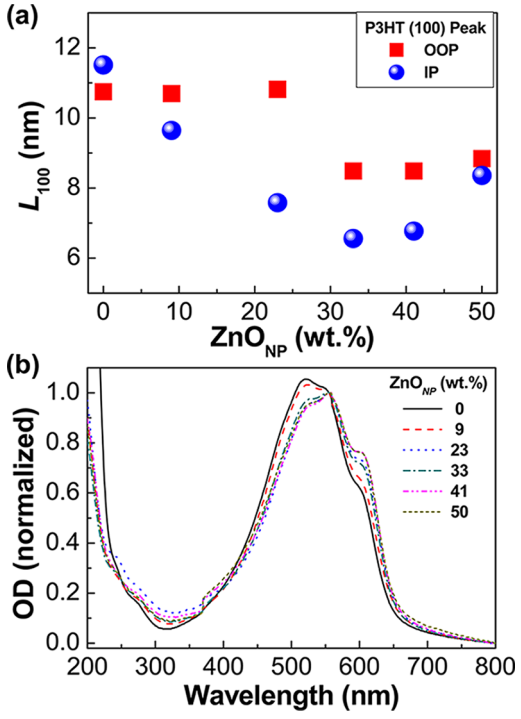

Figure 6. (a) Crystal size (L_{100}) of P3HT domains calculated from the 1D GIXD profiles from Figure 5b, c, (b) optical absorption spectra of the P3HT:ZnO_{NP} films coated on quartz substrates.

P3HTs in the P3HT:ZnO_{NP} films, which can be attributed to the charge transport in the films. In addition, it is noteworthy from the optical absorption spectra in Figure 6b that the overall degree of the P3HT chain stacking was enhanced by the presence of ZnO_{NP} though the weight fraction of P3HT was decreased as the ZnO_{NP} content increased. Hence we can briefly conclude that the high I_D trend in the output curves at high ZnO_{NP} contents (Figure 3a) is mainly attributed to the improved hole transport in the presence of adverse effect of rough morphology leading to an electrical leakage.

On the basis of the above results for the transistor characteristics in the dark, we examined the performance of HPTRs with the P3HT:ZnO_{NP} films by varying the incident light intensity (P_{IN}) at the wavelength of 555 nm. As shown in Figure 7, the I_D values in the output curves at V_G = −40 V were

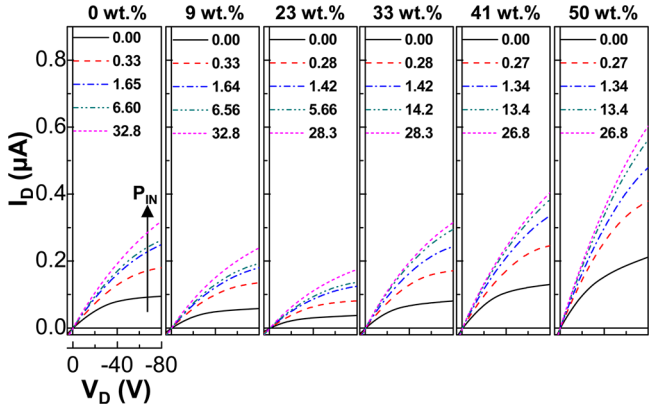

Figure 7. (a) Incident light intensity (P_{IN})-dependent output curves of the HPTRs with the P3HT:ZnO_{NP} films at V_G = −40 V. Arrow denotes the direction of P_{IN} increase. The numbers in the legends stand for P_{IN} values in $\mu W/cm^2$, while the ZnO_{NP} compositions are given in wt %.

increased by increasing P_{IN} irrespective of the ZnO_{NP} content, which supports that the present devices functioned properly as a phototransistor. Interestingly, we find that the I_D trend at the similar P_{IN} followed the trend in the dark. This implies that the performance of the present HPTRs is basically limited by their performances in the dark. Here we need to pay our attention to the fact that the I_D increment by illumination was higher for the HPTRs with the BHJ (P3HT:ZnO_{NP}) films at higher ZnO_{NP} contents than the device with the pristine P3HT film even though the amount of P3HT was lower for the BHJ films than for the pristine P3HT film. Thus we speculate that the efficient charge separation at the interfaces between the P3HT domains and the ZnO_{NP} domains in the BHJ films might overwhelm the lower P3HT content that could result in the lower efficiency of charge (exciton) generation. The enlarged output and transfer curves are given in Figure S4 in the Supporting Information, where we can see the gradual and huge shift (toward a positive V_G) in the threshold voltages with P_{IN} for all devices. The trend of output and transfer curves with P_{IN} was similar for other major absorption wavelengths of P3HT (see Figures S5 and S6 in the Supporting Information).

To further understand the P_{IN} dependency of I_D, the I_D values at a fixed voltage condition (V_G = −40 V and V_D = −80 V) were plotted as a function of I_D. As shown in Figure 8a, the I_D values were linearly increased with P_{IN} for all composition, which indicates that at a fixed ZnO_{NP} content both exciton generation and charge separation upon illumination were almost not affected by the P_{IN} variation. However, the slope (I_D/P_{IN}) was changed as the ZnO_{NP} content varied. The lowest

dx.doi.org/10.1021/am302765a | ACS Appl. Mater. Interfaces 2013, 5, 1385−1392

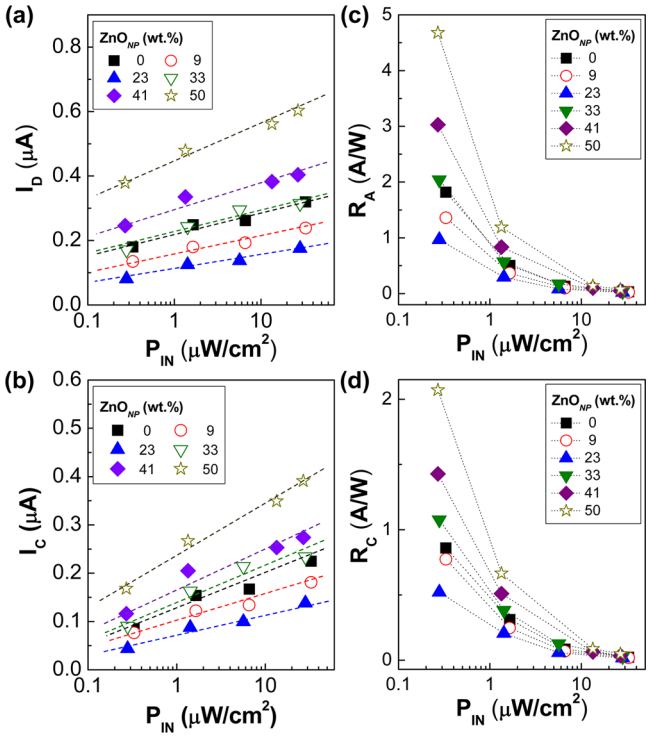

Figure 8. (a) Drain current (I_D) as a function of incident light intensity (P_{IN}) for the HPTRs with the P3HT:ZnO_{NP} films at V_G = −40 V and V_D = −80 V. (b) Corrected drain current (I_C) from I_D in (a) by subtracting the drain current in the dark. (c) Apparent responsivity (R_A) calculated from the uncorrected drain current (I_D). (d) Corrected responsivity (R_C) calculated from the corrected drain current (I_C). The slopes calculated in (a) and (b) (note that the slope for I_D/P_{IN} is the same for I_C/P_{IN}): I_D/P_{IN} ($\times 10^{-8}$ cm^2 A/W) = 6.6 (0 wt %), 5.0 (9 wt %), 4.5 (23 wt %), 7.3 (33 wt %), 7.9 (41 wt %), 11.0 (50 wt %).

slope was obtained at 23 wt %, whereas the highest slope was measured at 50 wt % (see exact values in the figure caption). This trend is almost in agreement with the trend in Figure 7, indicating that the rate (efficiency) of charge generation/separation in the present HPTRs did influence on the overall performance of devices which is dependent on the ZnO_{NP} content. The slope change with the ZnO_{NP} content was also observed for the corrected drain current (I_C) that reflects the true photocurrent without the field-effect current (Figure 8b). In terms of responsivity, both apparent (R_A) and corrected responsivities (R_C) exhibited a gradually decreasing trend with P_{IN} for all devices (Figure 8c,d). This result indicates that the responsivity of devices is reduced as increasing the population of excitons generated in the channel area, which can be ascribed to the increased charge recombination owing to the increased number of charge carriers (holes and electrons) even though the drain current could be enhanced by the larger number of charge carriers. The present trend of P_{IN}-dependent responsivity is in accordance with the previous reports.[31,33] The highest R_A and R_C values were obtained at 50 wt %, while the lowest responsivities were measured at 23 wt % regardless of P_{IN}. The highest R_A and R_C at 50 wt % under P_{IN} = 0.27 μW/cm^2 were 4.7 A/W and 2.07 A/W, respectively, which are comparable with commercial inorganic phototransistors.[54,55] The R_C trend for three representative P_{IN} ranges is summarized as a function of the ZnO_{NP} content in Figure 9 (see the linear relationship in Figure S7 in the Supporting Information). Considering the R_C trend according to the different P_{IN}, the present HPTRs are expected to be effective as an ultrasensitive detector in the fields of biomedical diagnostics, ultrasensitive spectroscopy, space technology, military defense systems, etc., because of their higher responsivity at lower light intensity.

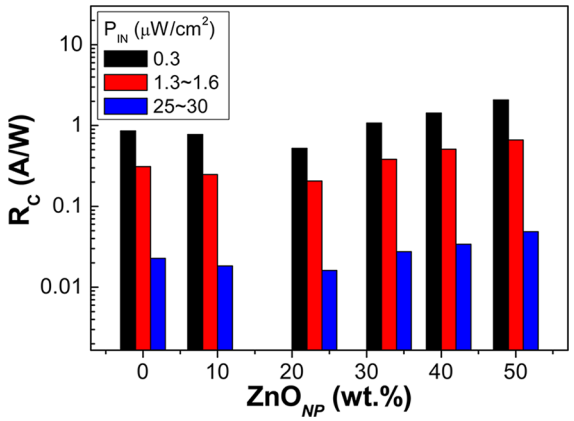

Figure 9. Corrected responsivity (R_C) as a function of the ZnO_{NP} content for the HPTRs with the P3HT:ZnO_{NP} films at V_G = −40 V and V_D = −80 V. Note that some data points were obtained by extrapolating from the actual measurement data points because of slightly different P_{IN} values (see Figure 8).

CONCLUSIONS

Hybrid phototransistors (HPTRs) were fabricated on glass substrates by employing organic/inorganic hybrid bulk heterojunction (BHJ) channel layers that are composed of p-type polymer (P3HT) and n-type inorganic nanoparticles (ZnO_{NP}). The HPTRs fabricated showed typical p-type transistor characteristics in the dark, even though the n-type ZnO_{NP} content increased up to 50 wt %. The lowest transistor performance was measured at 23 wt % ZnO_{NP} content, which has been assigned to the lowest hole mobility at this composition. However, the transistor performance was gradually enhanced by further increasing the ZnO_{NP} content (33−50 wt %) because of the improved charge separation at the BHJ interface between P3HT and ZnO_{NP} though the net P3HT content was lowered as the ZnO_{NP} content increased. The SEM and TEM measurements showed that the quality of the P3HT: ZnO_{NP} films was sufficient to support the proper functioning of devices. The GIXD measurement disclosed that the P3HT chain stacking/ordering was not seriously affected by the presence of ZnO_{NP} though the P3HT crystal size was varied by the ZnO_{NP} content. Upon illumination of monochromatic light, the drain current (I_D) was gradually increased as the incident light intensity (P_{IN}) increased due to the photocurrent generation in addition to the field-effect current. Interestingly, the lowest slope (I_D/P_{IN}) was measured at 23 wt %, whereas the highest slope was obtained at 50 wt %. This result was in accordance with the lowest performance of typical transistor performance, which supports the important aspect on the trade-off between optical absorption and BHJ formation. The highest apparent and corrected responsivities (R_A = 4.7 A/W and R_C = 2.07 A/W) were achieved for the HPTR with the P3HT:ZnO_{NP} film (50 wt % ZnO_{NP}) at P_{IN} = 0.27 μW/cm^2 (550 nm). Finally, further improvement is expected through optimization of device fabrication conditions (thermal annealing temperature/time, thickness, etc.) and use of various sized ZnO_{NP}, whereas a broadband hybrid phototransistor that detects

photons over wide wavelengths can be achieved by employing low band gap polymers.

■ ASSOCIATED CONTENT

Supporting Information

Transfer curves, enlarged 2D GIXD images, powder XRD profile, output and transfer curves under illumination at three major wavelengths (525, 555, and 605 nm), and corrected responsivity as a function of ZnO_{NP} content (linear scale). This material is available free of charge via the Internet at http://pubs.acs.org.

■ AUTHOR INFORMATION

Corresponding Author

*E-mail: ykimm@knu.ac.kr (Y.K.), khj217@knu.ac.kr (H.K). Tel: +82-53-950-5616.

Notes

The authors declare no competing financial interest.

■ ACKNOWLEDGMENTS

This work was financially supported by Korean Government grants (Basic Research Laboratory Program_2012-0008843, Pioneer Research Center Program_2012-0001262, Priority Research Center Program_2012-23460000, NRF_2012-000523, NRF_2011-0007085, NRF_2012-0004378, NRF_2012-027883).

■ REFERENCES

(1) Facchetti, A. *Chem. Mater.* **2011**, *23*, 733−758.
(2) Heimel, G.; Salzmann, I.; Duhm, S.; Koch, N. *Chem. Mater.* **2011**, *23*, 359−377.
(3) Wang, C.; Dong, H.; Hu, W.; Liu, Y.; Zhu, D. *Chem. Rev.* **2012**, *112*, 2208−2267.
(4) Kim, J.; Kim, S.; Rieke, R. *Macromol. Res.* **2011**, *19*, 749−752.
(5) Jung, Y.; Lee, S.; Sankaraiah, S.; Cheong, I.; Choi, W.; Kim, J. *Macromol. Res.* **2011**, *19*, 1114−1120.
(6) Tao, Y.; Yang, C.; Qin, J. *Chem. Soc. Rev.* **2011**, *40*, 2943−2970.
(7) Grimsdale, A. C.; Chan, K. L.; Martin, R. E.; Jokisz, P. G.; Holmes, A. B. *Chem. Rev.* **2009**, *109*, 897−1091.
(8) Kim, Y.; Ha, C. S. In *Advances in Organic Light-Emitting Device*; Trans Tech Publications: Zurich, Switzerland, 2008.
(9) Padinger, F.; Rittberger, R. S.; Sariciftci, N. S. *Adv. Funct. Mater.* **2003**, *13*, 85−88.
(10) Kim, Y.; Choulis, S. A.; Nelson, J.; Bradley, D. D. C.; Cook, S.; Durrant, J. R. *Appl. Phys. Lett.* **2005**, *86*, 063502.
(11) Li, G.; Shrotriya, V.; Huang, J.; Yao, Y.; Moriarty, T.; Emery, K.; Yang, Y. *Nat. Mater.* **2005**, *4*, 864−868.
(12) Kim, Y.; Cook, S.; Tuladhar, S. M.; Choulis, S. A.; Nelson, J.; Durrant, J. R.; Bradley, D. D. C.; Giles, M.; McCulloch, I.; Ha, C.-S.; Ree, M. *Nat. Mater.* **2006**, *5*, 197−203.
(13) Chen, H.; Hou, J.; Zhang, S.; Liang, Y.; Yang, G.; Yang, Y.; Yu, L.; Wu, Y.; Li, G. *Nat. Photon.* **2009**, *3*, 649−653.
(14) Dou, L.; You, J.; Yang, J.; Chen, C.; He, Y.; Murase, S.; Moriarty, T.; Emery, K.; Li, G.; Yang, Y. *Nat. Photon.* **2012**, *6*, 180−185.
(15) Heremans, P.; Gelinck, G. H.; Müller, R.; Baeg, K. J.; Kim, D. Y.; Noh, Y. Y. *Chem. Mater.* **2011**, *23*, 341−358.
(16) Naber, R. C. G.; Asadi, K.; Blom, P. W. M.; de Leeuw, D. M.; de Boer, B. *Adv. Mater.* **2010**, *22*, 933−945.
(17) Mas-Torrent, M.; Rovira, C. *Chem. Rev.* **2011**, *111*, 4833−4856.
(18) Ortiz, R. P.; Facchetti, A.; Marks, T. J. *Chem. Rev.* **2010**, *110*, 205−239.
(19) Tsao, H. N.; Cho, D. M.; Park, I.; Hansen, M. R.; Mavrinskiy, A.; Yoon, D. Y.; Graf, R.; Pisula, W.; Spiess, H. W.; Müllen, K. *J. Am. Chem. Soc.* **2011**, *133*, 2605−2612.
(20) Tanaka, H.; Yasuda, T.; Fujita, K.; Tsutsui, T. *Adv. Mater.* **2006**, *18*, 2230−2233.
(21) Peumans, P.; Yakimov, A.; Forrest, S. R. *J. Appl. Phys.* **2003**, *93*, 3693−3723.
(22) Oh, J.; Choi, J.; Luong, B.; Kim, N. *Macromol. Res.* **2010**, *18*, 8−13.
(23) Saragi, T. P. I.; Pudzich, R.; Fuhrmann, T.; Salbeck. *J. Appl. Phys. Lett.* **2004**, *84*, 2334−2336.
(24) Narayan, K. S.; Kumar, N. *Appl. Phys. Lett.* **2011**, *79*, 1891−1893.
(25) Choi, M. C.; Kim, Y.; Ha, C. S. *Prog. Polym. Sci.* **2008**, *33*, 581−630.
(26) Noh, Y. Y.; Kim, D. Y.; Yase, K. *J. Appl. Phys.* **2005**, *98*, 074505.
(27) Mukherjee, B.; Sim, K.; Shin, T. J.; Lee, J.; Mukher-jee, M.; Ree, M.; Pyo, S. *J. Mater. Chem.* **2012**, *22*, 3192−3200.
(28) Singh, T. B.; Koeppe, R.; Sariciftci, N. S.; Morana, M.; Brabec, C. J. *Adv. Funct. Mater.* **2009**, *19*, 789−795.
(29) Dong, H.; Li, H.; Wang, E.; Nakashima, H.; Torimitsu, K.; Hu, W. *J. Phys. Chem. C.* **2008**, *112*, 19690−19693.
(30) Marjanović, N.; Singh, T. B.; Dennler, G.; Günes, S.; Neugebauer, H.; Sariciftci, N. S.; Schwödiauer, R.; Bauer, S. *Org. Electron.* **2006**, *7*, 188−194.
(31) Wasapinyokul, K.; Milne, W. I.; Chu, D. P. *J. Appl. Phys.* **2009**, *105*, 024509.
(32) Peet, J.; Soci, C.; Coffin, R. C.; Nguyen, T. Q.; Mi-khailovsky, A.; Moses, D.; Bazan, G. C. *Appl. Phys. Lett.* **2006**, *89*, 252105.
(33) Hwang, H.; Kim, H.; Nam, S.; Bradley, D. D. C.; Ha, C. S.; Kim, Y. *Nanoscale* **2011**, *3*, 2275−2279.
(34) Yang, S.; Zhao, N.; Zhang, L.; Zhong, H.; Liu, R.; Zou, B. *Nanotechnology* **2012**, *23*, 255203.
(35) Lee, K. H.; Park, C. H.; Lee, K.; Ha, T.; Kim, J. H.; Yun, J.; Lee, G. H.; Im, S. *Org. Electron.* **2011**, *12*, 1103−1107.
(36) Meixner, R. M.; Göbel, H.; Yildirim, F. A.; Bauhofer, W.; Krautschneider, W. *Appl. Phys. Lett.* **2006**, *89*, 092110.
(37) Kim, Y. S.; Bae, S. Y.; Kim, K. H.; Lee, T. W.; Hur, J. A.; Hoang, M. H.; Cho, M. J.; Kim, S. J.; Kim, Y.; Kim, M.; Lee, K.; Lee, S. J.; Choi, D. H. *Chem. Commun.* **2011**, *47*, 8907−8909.
(38) Cho, M. Y.; Kim, S. J.; Han, Y. D.; Park, D. H.; Kim, K. H.; Choi, D. H.; Joo, J. *Adv. Funct. Mater.* **2008**, *18*, 2905−2912.
(39) Guo, Y.; Du, C.; Di, C. A.; Zheng, J.; Sun, X.; Wen, Y.; Zhang, L.; Wu, W.; Yu, G.; Liu, Y. *Appl. Phys. Lett.* **2009**, *94*, 143303.
(40) Rogalski, A.; Adamiec, K.; Rutkowski, J. In *Narrow-Gap Semiconductor Photodiodes*; SPIE Press: Bellingham, WA, 2000.
(41) Mok, S. M.; Yan, F.; Chan, H. L. W. *Appl. Phys. Lett.* **2008**, *93*, 023310.
(42) Xu, Z. X.; Roy, V. A. L.; Stallinga, P.; Muccini, M.; Toffanin, S.; Xiang, H. F.; Che, C. M. *Appl. Phys. Lett.* **2007**, *90*, 223509.
(43) Schneider, J. J.; Hoffmann, R. C.; Engstler, J.; Soffke, O.; Jaegermann, W.; Issanin, A.; Klyszcz, A. *Adv. Mater.* **2008**, *20*, 3383−3387.
(44) Nam, S.; Kim, J.; Lee, H.; Kim, H.; Ha, C. S.; Kim, Y. *ACS Appl. Mater. Interfaces* **2012**, *4*, 1281−1288.
(45) Brédas, J. L.; Beljonne, D.; Coropceanu, V.; Cornil, J. *Chem. Rev.* **2004**, *104*, 4971−5003.
(46) Wenger, O. S. *Chem Soc. Rev.* **2011**, *40*, 3538−3550.
(47) Clarke, T. M.; Durrant, J. R. *Chem. Rev.* **2010**, *110*, 6736−6767.
(48) Kim, J.; Nam, S.; Jeong, J.; Kim, H.; Kim, Y. *J. Kor. Phys. Soc.* **2012**, *61*, 234−238.
(49) Yang, C.; Orfino, F. P.; Holdcroft, S. *Macromolecules* **1996**, *29*, 6510−6517.
(50) Sirringhaus, H.; Brown, P. J.; Friend, R. H.; Nielsen, M. M.; Bechgaard, K.; Langeveld-Voss, B. M. W.; Spiering, A. J. H.; Janssen, R. A. J.; Meijer, E. W.; Herwig, P.; de Leeuw, D. M. *Nature* **1999**, *401*, 685−688.
(51) Shin, M.; Kim, H.; Park, J.; Nam, S.; Heo, K.; Ree, M.; Ha, C.-S.; Kim, Y. *Adv. Funct. Mater.* **2010**, *20*, 748−754.
(52) Nam, S.; Shin, M.; Kim, H.; Kim, Y. *Nanoscale* **2010**, *2*, 2384−2389.

(53) Chiu, M.; Jeng, U.; Su, C.; Liang, K. S.; Wei, K. *Adv. Mater.* **2008**, *20*, 2573−2578.
(54) Kaneko, Y.; Koike, N.; Tsutsui, K.; Tsukada, T. *Appl. Phys. Lett.* **1990**, *56*, 650−652.
(55) Choi, C. S.; Kang, H. S.; Choi, W. Y.; Kim, H. J.; Choi, W. J.; Kim, D. J.; Jang, K. C.; Seo, K. S. *IEEE Photon. Technol. Lett.* **2003**, *15*, 846−848.